Hindawi
Mathematical Problems in Engineering
Volume 2023, Article ID 7825964, 11 pages
https://doi.org/10.1155/2023/7825964

Research Article

Simulation Analysis of Electromagnetic-Fluid-Temperature Field in Cable Shafts of High-Rise Buildings

Bo Qu,[1] Xin Li,[1] Xing-yao Xiang,[1] Shao-wei Wu,[1] Kai Li ,[2] Xin Li,[2] and Zhi-cong Zheng[3]

[1]*State Grid Hubei Electric Power Co., Ltd., Shiyan Power Supply Company, Shiyan 442099, China*
[2]*Information Engineering School of Nanchang University, Nanchang 330031, China*
[3]*College of Electrical Engineering and Automation, Fuzhou University, Fuzhou 350108, China*

Correspondence should be addressed to Kai Li; 416100210367@email.ncu.edu.cn

Received 5 August 2022; Revised 6 October 2022; Accepted 19 April 2023; Published 8 May 2023

Academic Editor: Ji Wang

High-rise building fires can be characterized by a rapid spreading and are challenging to extinguish. The chimney effect of cable shafts in high-rise buildings will greatly increase the spread speed of fire and smoke, and will also make it harder to put out fires. Therefore, fire-blocking materials or fire protection measures are usually used in cable shafts to slow down or even block the spread of fire. Currently, most of the research focuses on the fire performance of fire protection materials, and there are relatively few studies on the impact of fire-blocking materials on the operation state of cables. Based on the theories of electromagnetism, fluid mechanics, and thermodynamics, the paper establishes a multiphysics simulation model of a double-layer cable shaft. Then, the electromagnetic-fluid-temperature distribution in the cable shaft under rated operating conditions is analyzed, and the influence of the fire-blocking material is discussed. The simulation results show that the firestop material will affect the heat dissipation of the cable, which causes the hot-spot temperature of the cable to slightly increase by 1 to 2°C, and the relative growth rate of its hot-spot temperature rise is close to 6.83%.

1. Introduction

With the development of the social economy, the number of high-rise buildings and superhigh-rise buildings is increasing day by day. They can effectively improve the utilization of land, but will also inevitably increases the potential risk and danger of fire [1, 2]. During the construction of high-rise buildings, a large number of pipes pass through the walls or floors of the building and leave holes or gaps that will provide favorable conditions for the spread of fire. For example, the chimney effect of cable shafts can cause the rapid spread of smoke, and also increases the hazard of fire and the difficulty of extinguishing [3, 4]. To reduce the risk of fire in high-rise buildings as much as possible, relevant departments in my country have published a series of standards, and have made corresponding regulations on fire-blocking measures or materials [5–8]. At the same time, many scholars have also carried out a lot of research work on the fire-blocking of high-rise buildings and achieved certain results [3, 4, 9–11]. Based on existing research results, it can be found that the current research presents the following characteristics: (1) most of the research objects focus on cables laid in cable trenches or tunnels in substations [12–15]; (2) researchers pay more attention to the effect of cable fire-blocking materials. The effect of blocking materials on the spread of fire is often studied, while the effect of fire-blocking materials on the operation state of cables is relatively rare [9, 11, 12]. For example, by considering the gap in the firewall of the high-voltage cable trench of the substation, the spread mode of fire and smoke before and after adding the firestop material was comparatively studied in [12]. Based on fire dynamics simulation, the fire development process of the cable under single-phase grounding fault condition was studied, and the fire risk assessment is carried out [13]. In the literature [14], a cable combustion test was designed and established to analyze the fire propagation process of electric cables, and the influence of vertical cable shafts on fire propagation was also studied. In the literature

[16], a multiphysics simulation model of the cable shaft is established in this paper. Through the simulation analysis of the transient electromagnetic-fluid-temperature field, the temperature change of the cable is obtained. By changing the plugging material parameters, the influence of different plugging materials on the electromagnetic-fluid-temperature field of cable under normal operation is simulated. Overall, there are fewer relevant studies on cable shafts in high-rise buildings and even fewer analysis studies on the internal operation status of cable shafts, which is of great significance to the operation and maintenance management of power cables.

Therefore, the paper builds a three-dimensional simulation model of a two-layer vertical cable shaft, and the electromagnetic-fluid-temperature field analysis was carried out. Then, the influence of the firestop material on the operation state of power cables was discussed, which can provide a reference for the evaluation of the firestop material performance of the cable shafts in a high-rise building.

2. Simulation Theory

The temperature distribution in the cable shaft can be obtained by solving the control equations of the electromagnetic field, fluid field, and temperature field.

2.1. Electromagnetic Field Formula. The heat generated by an electric current through a conductor, the Joule effect, is the main reason for the heating of power equipment such as cables and transformers. The Joule heat can be calculated by the electromagnetic field analysis, and it is also the load of the fluid-temperature field analysis at the same time. Therefore, the electromagnetic field solution of the cable shaft model is mainly based on Maxwell's equations, which are used to solve the Joule heat loss generated during the operation of the cable. The governing equations are as follows [17, 18]:

$$\begin{cases} \nabla \times \mathbf{E} + \dfrac{\partial \mathbf{B}}{\partial t} = 0, \\ \nabla \times \mathbf{H} = \mathbf{Js}, \\ \nabla \cdot \mathbf{E} = \dfrac{\rho}{\varepsilon 0}, \\ \nabla \cdot \mathbf{B} = 0, \end{cases} \tag{1}$$

where **B**, **H**, and **E** are the magnetic flux density, magnetic field strength, and electric field strength, the unit of **B** is T, the unit of **H** is A/m, the unit of **E** is V/m, respectively, and $\mathbf{B} = \mu\mathbf{H}$; μ is the magnetic permeability, the unit is H/m; $\mathbf{J_s}$ is the current density flowing through the cable core, and $\mathbf{J_s} = \sigma \mathbf{E}$, the unit is A/m^2; σ is the electrical conductivity, the unit is S/m.

2.2. Temperature Field Formula. With the influence of Joule heat induced by the electromagnetic field, the temperature of the cable will gradually increase, and it will spread from the cable core to the outer insulating sheath, and finally, spread to the surrounding air. To simulate the above process, this paper will carry out the transient temperature field solution analysis, which will reflect the relationship between the cable temperature and the operating time. Therefore, based on the principle of heat transfer, the above heat transfer process mainly involves heat conduction and convection, and the heat radiation of the cable sheath is ignored in the paper. The governing equations of thermal analysis are as follows [19–22]:

2.2.1. Heat Conduction. Heat conduction is mainly used to describe the temperature change process of the cable body under the action of Joule heat.

$$q = -kS\frac{\partial T}{\partial x}, \tag{2}$$

where q is the heat flux per unit area, which unit is J/m^2. K is the thermal conductivity, which unit is W·m^{-1}·K^{-1}. S is the area in the vertical direction of the heat flux density, which unit is m^2. $\partial T/\partial x$ is the temperature gradient in the heat flow direction, which unit is K/m. The negative symbol in equation (2) means that the direction of heat flux is always positive with the temperature gradient.

2.2.2. Heat Convection. Thermal convection is mainly used to describe the convective heat transfer process between the surface of the cable-insulating sheath and the surrounding air.

$$q = hS(T - Tf), \tag{3}$$

where h is the convective heat transfer coefficient, which unit is W·m^{-2}·K^{-1}. S is the surface area of the wall, which unit is m^2. T and T_f are the temperatures of the wall and the external fluid, respectively, which units are °C. This formula is mainly used to describe the heat transfer between the solid wall and the fluid.

2.3. Fluid Field Formula. During the operation of the cable, the temperature of the cable gradually increases, and the temperature difference between itself and the surrounding air will appear. Once the temperature difference occurs, the airflow on the surface of the cable will intensify, and the airflow will in turn affect the temperature distribution of the cable. In this phenomenon, there is an interaction between the fluid field and the temperature field. The solution of the fluid problem mainly depends on the establishment of computational fluid dynamics, and the mathematical model of the flow and heat transfer of the heat dissipation medium in the fluid field is mainly based on three conservation equations: the mass conservation equation, the momentum conservation equation, and the energy conservation equation. The governing equations are as follows [18]:

$$\begin{gathered} \nabla \cdot \mathbf{v} = 0, \\ \frac{\partial(\rho \mathbf{v})}{\partial t} + \rho \mathbf{v} \nabla \mathbf{v} = \rho f - \nabla \mathbf{p} + u\nabla^2 \mathbf{v}, \\ \frac{\partial(\rho e)}{\partial t} + \nabla \cdot (\rho e \mathbf{v}) = \rho \mathbf{q} - \nabla(k\nabla T) + q, \end{gathered} \tag{4}$$

where ρ is the density of the air, $\mathbf{v}$ is the flow velocity of the air, f is the volume force of the fluid, $\mathbf{q}$ is the volume heat source of the fluid, and c is the specific heat capacity.

2.4. Multiphysics Coupling Analysis Methods. According to the different coupling methods between the physical fields, the multiphysics coupling methods can be divided into two types: direct coupling and indirect coupling mode. Among them, the direct coupling method can be divided into the one-way coupling and the two-way coupling mode. For example, in the simulation of this paper, the influence between temperature distribution, Joule heat, and fluid flow velocity must be considered in two-way coupling. The indirect coupling method solves each physical field in turn and uses the simulation result of the previous physical field as the loading condition of the next physical field, which also means that it is impossible to consider the effect of the next physical field on the previous physical field. Therefore, compared with the indirect coupling method, the direct coupling method can fully consider the interaction between different physical fields, and the simulation results will also be much closer to the actual situation.

Considering that the simplified multiphysics model of the cable shafts is not complicated, the direct coupling solution method is adopted in this paper. The electromagnetic field, fluid field, and temperature field are solved simultaneously in the simulation model, as shown in Figure 1. The interaction and coupling effects between these physical fields are considered. The convergence condition of the simulation is mainly based on the temperature distribution of the cable shaft, that is to say, when the temperature distribution meets the preset conditions, the simulation will stop.

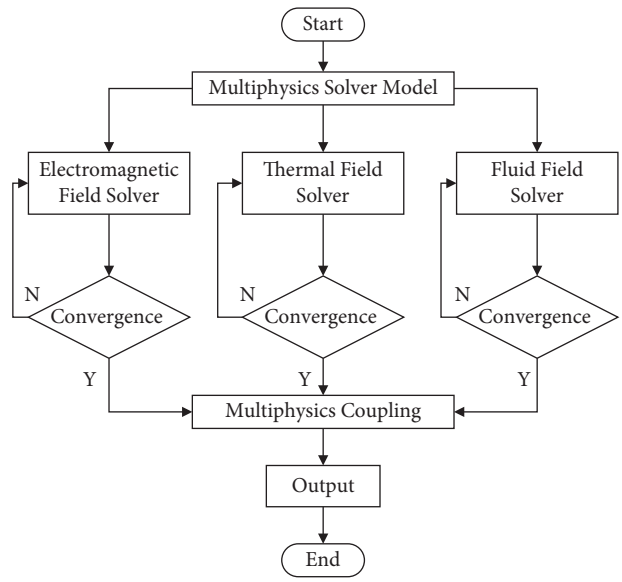

Figure 1: Electromagnetic-fluid-thermal coupled analysis method.

3. Multiphysics Simulation Model

3.1. Simulation Model of Cable Shaft. In this paper, a multiphysics simulation model is constructed by taking the double-layer cable shaft as the research object. In consideration of the difficulty of multiphysics analysis and the requirements for solution accuracy in the paper, the simulation model is simplified in several parts, which include the following:

(i) Considering that the hot-spot area of the power cable is mainly located at the junction of the upper and lower layers of the cable shaft, the height of the upper cable shaft is lowered to reduce the size of the model and the total amount of model mesh.

(ii) Structures such as the door of the cable shaft and the air gap between the cable and cable shaft are not considered in the model. That is to say, the cable shaft door is in a completely closed state, ignoring the convective diffusion between the cable shaft and the outside of the shaft.

(iii) The power cable studied in the paper is a VV-0.6/1 kV PVC-insulated three-core power cable, and its rated current is 113 A. The cross-sectional area of the cable conductor is 50 mm^2, and the outer diameter of the cable is 30 mm. The 1 kV three-core cable consists of the cable conductor, semiconductor shielding layer, inner sheath, insulating filler material, and outer sheath. Taking into account the huge difference in the size of cables versus cable shafts, the cable model is simplified into two parts, which include the cable conductor and the outer sheath. At the same time, the structural parameters of the cable conductor and sheath are equivalently and calculated in order to ensure the accuracy of simulation and reduce the number of meshes for the cable model.

(iv) The firestop material is mainly used to block the air gap between the cable and the middle floor of the cable shaft. Therefore, the gap between the fire-blocking material and the floor caused by poor construction or other reason is not considered, that is to say, the firestop material completely blocks the air gap and blocks the airflow between the upper and lower cable shafts.

According to the cable shaft structure of a high-rise building, a multiphysics simulation model of the cable shaft is established, as shown in Figure 2. The external dimensions of the cable shaft model are 1880 mm × 1680 mm × 3720 mm. The height of the lower floor is 2300 mm. The wall thickness is 240 mm, and the middle floor wall thickness is 120 mm. At the same time, eight and six 1 kV polyethylene sheathed three-core cables are arranged at the center of the walls on the left and right sides of the cable shaft, respectively. The distance between adjacent cables is 50 mm, and the distance between the center of the cable on the left and right sides of the wall is 200 mm and 150 mm, respectively.

3.2. Model Parameters. The parameters of the simulation model mainly include material parameters, boundary conditions, excitation conditions, and solve settings in each

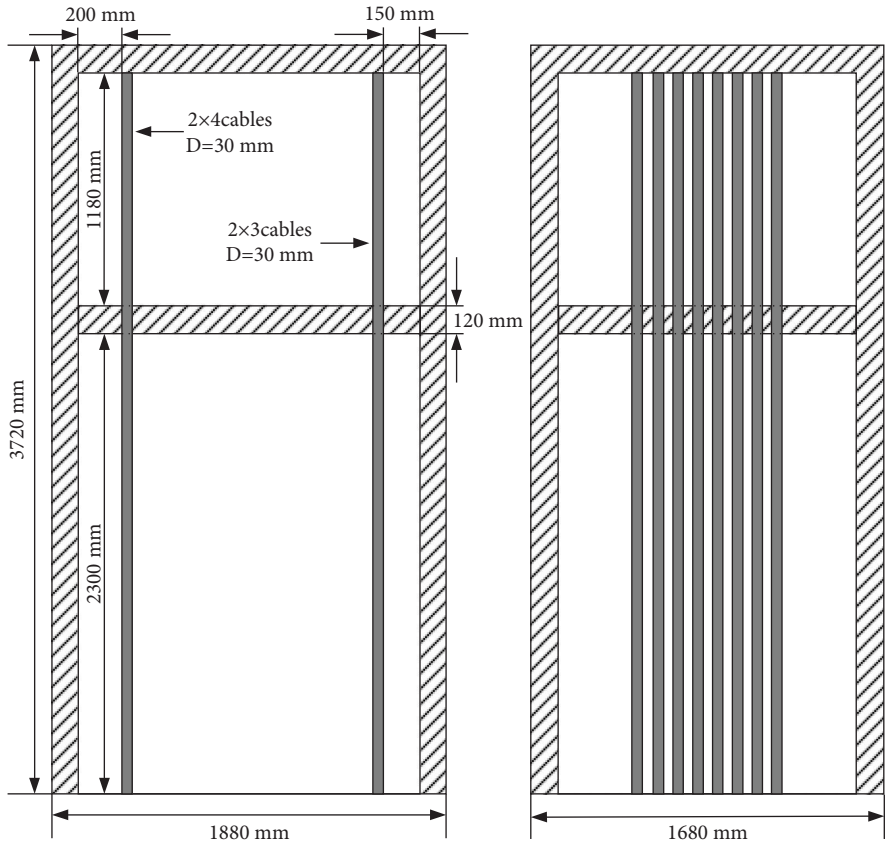

Figure 2: The simulation model of cable shaft. (a) The front view. (b) The side view.

physical field. As the direct coupling method is used in this paper, the settings of the above parameters can be accomplished in the simulation model at the same time. While for the convenience of description, the parameter settings of the electromagnetic field, fluid field, and temperature field are introduced separately here.

3.2.1. Electromagnetic Field Parameters. In the electromagnetic field, the relative permeability of each part of the model is set to 1, the resistance of the cable core per unit length is set to 0.387 Ω/km, and the effect of temperature on the resistivity is also considered.

3.2.2. Fluid Field Parameters. In the solution of the fluid field, the flow characteristics of the air inside the cable shaft are mainly considered. The velocity of airflow is closely related to the temperature distribution inside the cable shaft. The parameters such as air density and thermal conductivity are related to temperature, which is needed to be considered in the paper. The relationship between the material parameters of the air and the temperature is considered, as shown in Table 1.

3.2.3. Temperature Field Parameters. In the solution of fluid and temperature field, the material parameters mainly include the thermal conductivity, specific heat capacity, and density of solid media such as cable conductor, outer sheath, and concrete, as shown in Table 2.

For the air in the cable shaft, in addition to the above material parameters, it is also necessary to consider the dynamic viscosity used to describe the airflow and consider the change law between its physical parameters and temperature, as shown in Table 1.

3.2.4. Excitation and Boundary Conditions. In terms of electromagnetic field loading conditions, a voltage drop of 0.158 V is loaded at the head and end of the cable to simulate the current flowing in the cable. The phase difference between different cables is also taken into account in the paper. For the solution of the fluid-temperature field, the initial temperature of the model is set to 20.0°C. At the same time, the boundary temperature on the outer wall of the cable shaft is set to 20.0°C.

3.2.5. Other Parameters. The transient coupling electromagnetic-fluid-temperature field in the paper is calculated by COMSOL, and the transient solver is used. The total simulation time is set to 24 hours, and the transient solution time step is 0.1 hours. At the same time, the convergence condition of the solution error is set as the temperature difference between adjacent solution steps is less than 0.1°C; that is, when either the model simulation time or the solution error meets the above convergence conditions, the simulation ends.

Table 1: Parameters of fluid simulation.

Materials	Parameters	Values
Air	Thermal conductivity ($W \cdot m^{-1} \cdot K^{-1}$)	$-8.383 \times 10^{-7} + 8.36 \times 10^{-8}\,T$
	Specific heat capacity ($J \cdot kg \cdot K^{-1}$)	$1047.64 - 0.373\,T + 9.45 \times 10^{-4}\,T^2$
	Density ($kg \cdot m^{-3}$)	$3.102 - 0.009\,T + 8.614 \times 10^{-6}\,T^2$
	Dynamic viscosity (Pa·s)	$-8.383 \times 10^{-7} + 8.36 \times 10^{-8}\,T$

Table 2: Parameters of thermal simulation.

Materials	Parameters	Values
Copper	Thermal conductivity ($W \cdot m^{-1} \cdot K^{-1}$)	400
	Specific heat capacity ($J \cdot kg \cdot K^{-1}$)	385
	Density ($kg \cdot m^{-3}$)	8960
Polyethylene	Thermal conductivity ($W \cdot m^{-1} \cdot K^{-1}$)	0.231
	Specific heat capacity ($J \cdot kg \cdot K^{-1}$)	2300
	Density ($kg \cdot m^{-3}$)	960
Concrete	Thermal conductivity ($W \cdot m^{-1} \cdot K^{-1}$)	1.28
	Specific heat capacity ($J \cdot kg \cdot K^{-1}$)	880
	Density ($kg \cdot m^{-3}$)	2350

4. Simulation Results

Based on the above simulation model and simulation parameters, the electromagnetic-fluid-temperature field coupling analysis of the cable shaft model was carried out. The simulation results of the temperature and fluid distribution of the cable shaft are as follows.

4.1. Simulation Results of Temperature Field. For the simulation model without firestop material, the temperature distribution inside the cable shaft under steady state is shown in Figure 3. The simulation results show that under the normal operation state of the cable, the hot-spot temperature inside the cable shaft is 40.50°C, and the temperature rise of the hot-spot is 20.5°C. For the lower and upper cable shafts, the overall temperature distribution increases gradually with the height of the cable and finally decreases slightly near the top floor.

Combined with the above simulation results, the transverse and longitudinal sectional results at the center of the cable shaft, respectively, are obtained, as shown in Figure 4. It can be seen that the maximum temperature of the air in the lower layer of the cable shaft is slightly lower than the cable hot-spot temperature. In addition to the air between these power cables, the temperature of the air at the top of the cable shaft also exceeds 30.0°C.

The cross-sectional results of the cable shaft at the position where the hot-spot temperature of the cable occurs are also obtained. The temperature distribution of the section of the simulation model is shown in Figure 5. The simulation results show that, except for the power cables and the air close to the cables, the temperature in other areas of the cable shaft is relatively low. As the distance between the air and the surface of the cable increases, the temperature tends to decrease rapidly. The maximum air temperature at this height is roughly about 28.0°C. In addition, it should be noted that due to the huge difference in the model size between the power cable and cable shaft, the meshing of the cables cannot be controlled to a very small size. These results in a noncircular cross-section of cables in Figure 5, while in reality, the cables in the model are all cylinders.

Take the three positions where the maximum temperature occurs in Figures 3 and 4 as the observation points, respectively, the variation curves of the temperature at these sampling points are shown in Figure 6. The simulation results show that the variation trends of the temperature curves are similar. As the simulation time increases, the temperature gradually increases, but the increase will slow down at the same time and eventually reach the final steady state. When the simulation time reaches 4 to 5 hours, that is, after the cable has been running under the rated load for 4 to 5 hours, the temperature rise of the cable shaft has gradually slowed down.

In addition to the temperature curve at the above special points, the temperature distribution at different locations inside the cable shaft should also be paid attention to. On the one hand, it is necessary to understand the temperature change relationship at different locations; on the other hand, the changing relationship may be related to time. Therefore, the temperature distribution inside the cable shaft corresponding to different times of the above curve is obtained, as shown in Figure 7. The simulation results show that with the increase of the running time, the position where the hot-spot temperature occurs remains unchanged, but the temperature difference between the different cables and between the cables and the surrounding air gradually increases. According to the cable temperature change curve, the hot-spot temperature has increased to 34.36°C within the first 1.5 hours, that is, the temperature rise has reached about 70.0% of the hot-spot temperature rise. With the increase of time, the heating effect of the cable on the surrounding air appears which eventually leads to an increase in the air temperature at the top of the lower cable shaft.

4.2. Simulation Results of Fluid Field. The distribution of the fluid field in the cable shaft is not directly related to the running state of the cable. The heat generated by the operation of the cable affects the air flow inside the cable shaft, which in turn is conducive to the heat dissipation of the cable. This air flow varies as the cable temperature changes, but will also reach a steady state as the temperature stabilizes. Based on the multiphysics simulation results, the air velocity distribution of the transverse and longitudinal sections inside the cable shaft is shown in Figure 8.

As can be seen from Figure 8, except for the air very close to the cable, the air velocity at the bottom of the cable shaft is not significant, and the areas with faster air flow are mainly

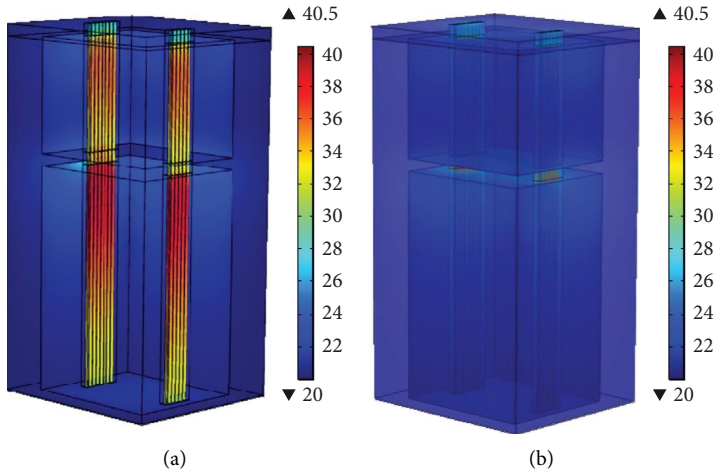

Figure 3: Thermal distribution inside the cable shaft. (a) Internal part. (b) External part.

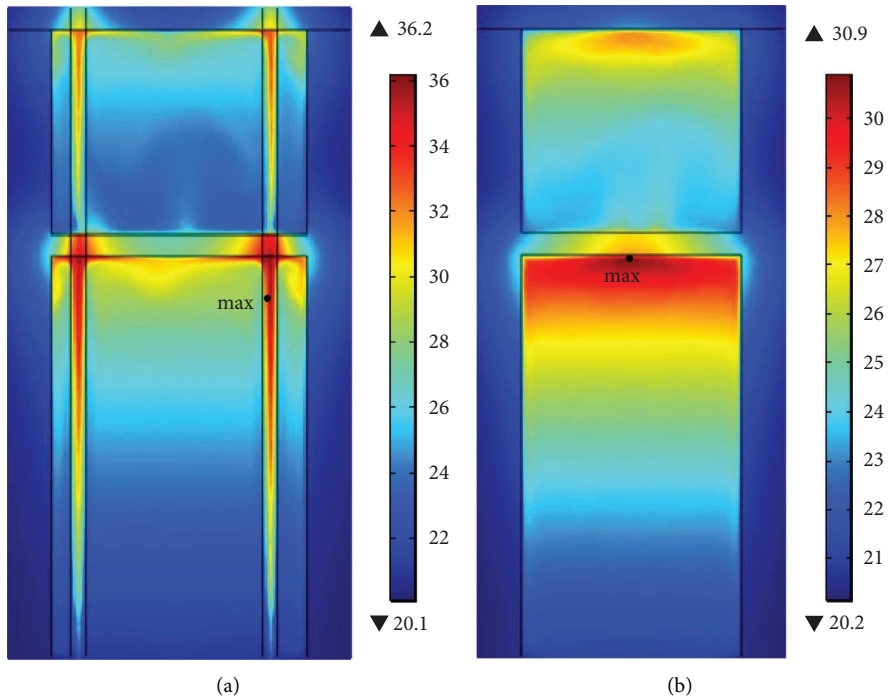

Figure 4: Sectional temperature distribution of the cable shaft. (a) Transverse section. (b) Longitudinal section.

concentrated below the middle floor. For the lower cable shaft, the air around the cable moves upwards and then moves downwards after being blocked by the floor slab in the middle of the cable shaft. On the contrary, the air velocity of the upper cable shaft is much larger, for example, the air in the area right above the middle floor slab. This area is shown in the results in Figure 4(b) with a very low temperature, which reflects the heat dissipation effect of the airflow on this region is very significant.

Taking the position where the maximum air velocity occurs in Figure 8 as the observation point, the variation curve of the air velocity at the sampling point is shown in Figure 9. It can be found that the airflow rate increase rapidly and then slowly reaches a steady state after a slight decrease. Combined with the temperature curve in Figure 6, the airflow rate is mainly related to change trend of the temperature. When the temperature increases rapidly, the airflow rate also increases accordingly. Finally, when the air velocity stabilizes, the temperature of the cable also reaches a stable state.

5. Discussion on the Effect of Fire-Blocking Materials

To study the effect of firestop material on the operation state of the cable, the air gap between the cable and the middle floor slab in the simulation model shown in Figure 3 is replaced by the sealing material. The physical parameters of

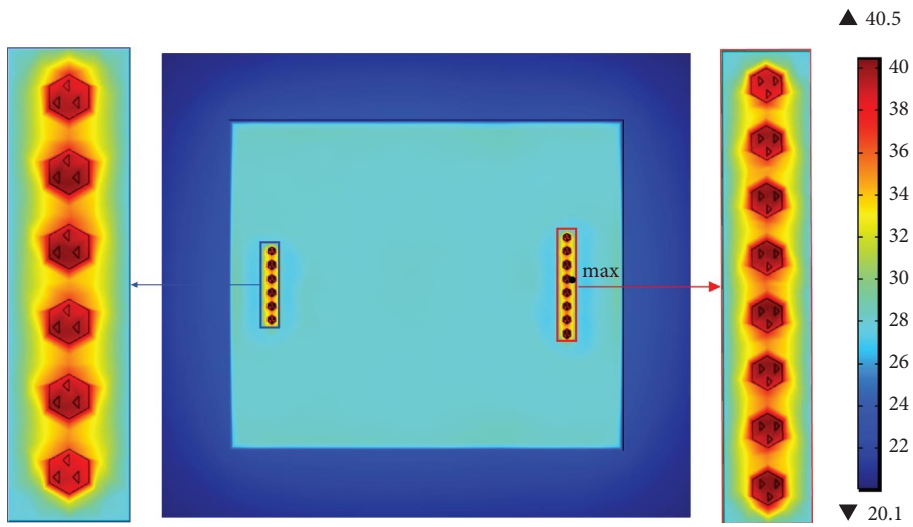

Figure 5: Sectional temperature distribution of the cable shaft (hot-spot location).

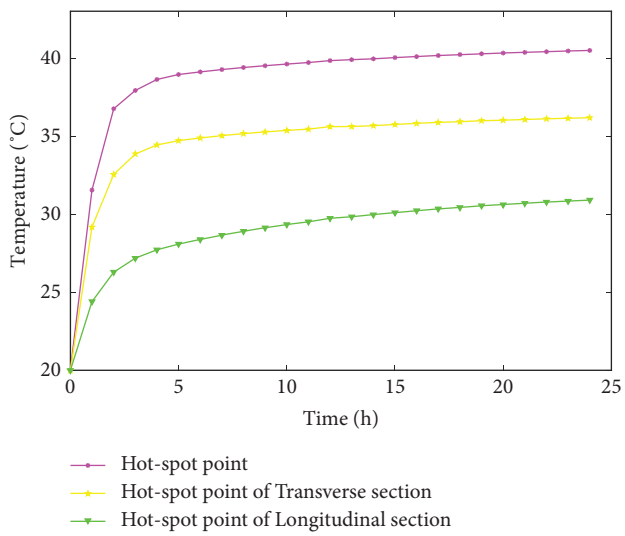

Figure 6: Temperature curve of the sampling points.

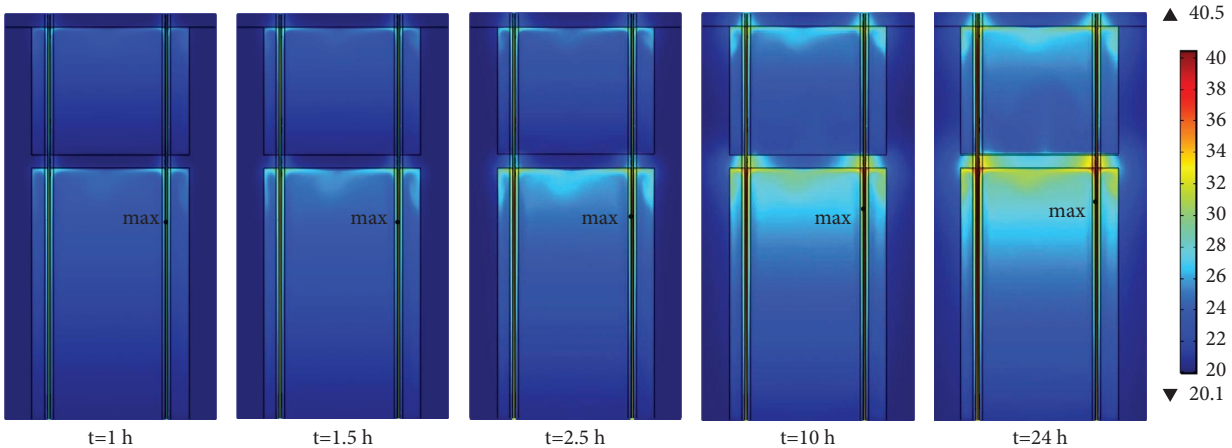

Figure 7: Temperature distribution inside the cable at different simulation times.

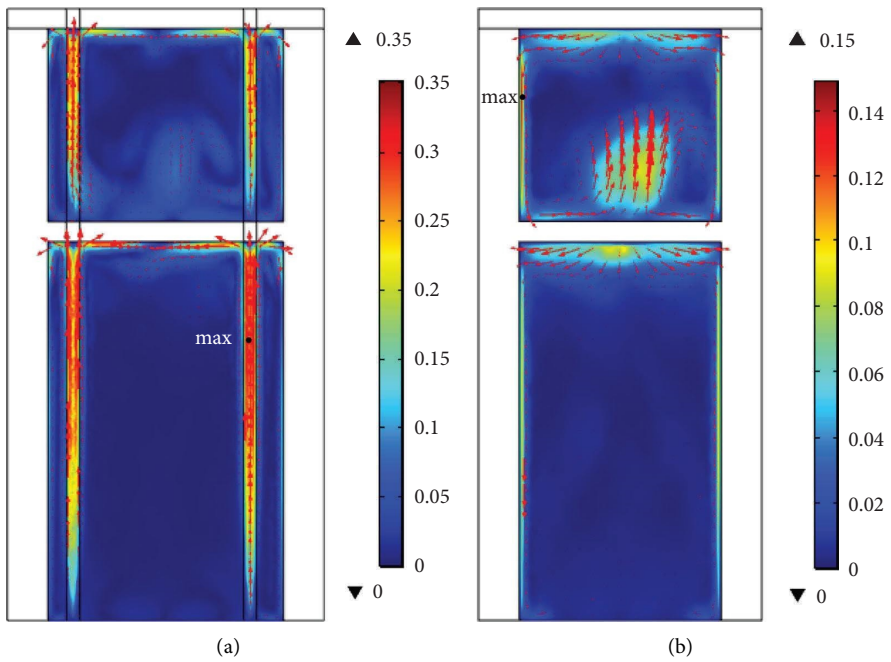

Figure 8: Sectional distribution of air velocity in cable shaft. (a) Transverse section. (b) Longitudinal section.

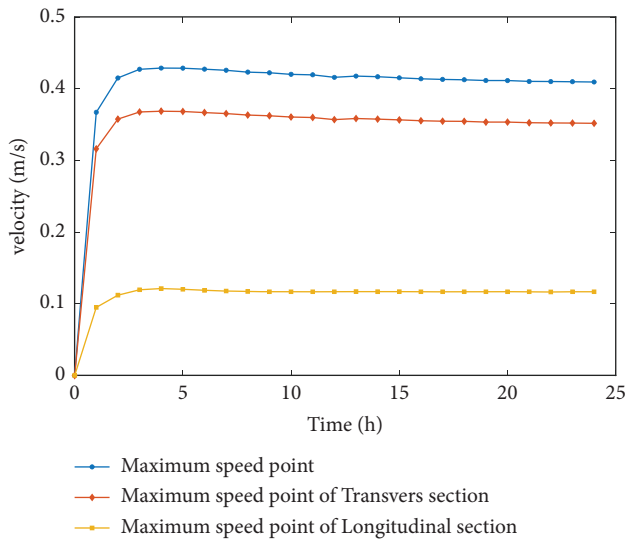

Figure 9: Air velocity curve of the sampling point.

Table 3: Parameters of firestop material.

Materials	Parameters	Values
Firestop material	Thermal conductivity ($W \cdot m^{-1} \cdot K^{-1}$)	0.042
	Specific heat capacity ($J \cdot kg \cdot K^{-1}$)	850
	Density ($kg \cdot m^{-3}$)	73

Figure 10: Thermal distribution inside the cable shaft (with firestop material).

the firestop materials in the simulation model are shown in Table 3. Except for the above parameters, the rest of the model and the simulation conditions remain the same compared to the model in Section 3.

Figure 10 shows the temperature distribution inside the cable shaft after the fire-blocking materials are used. Comparing the results in Figures 3 and 10, it can be found that under rated operating conditions, the hot-spot temperature of the cable increases from 40.50°C to 41.90°C. The application of firestop materials in the paper has led to an increase in the hot-spot temperature by 1.4°C, and the relative change of the hot-spot temperature rise is 6.83%. In addition to the increase in hot-spot temperature, the overall temperature increase of the upper and lower cables is also obvious, especially since the temperature of the cable blocked by the firestop material is close to 10.0°C. For the 1 kV PVC-insulated power cable studied in the paper, its long-term allowable operating temperature is 70°C. According to the simulation results in this paper, the running state of the cable is safe before and after adding fireproof materials. However, it should be noted that if the ambient temperature increases or the operating current of

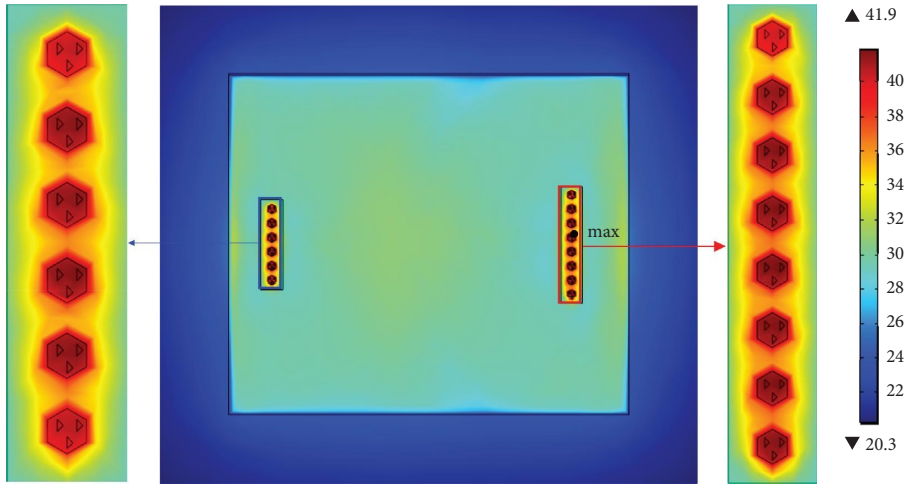

Figure 11: Sectional temperature distribution of the cable shaft (with firestop material).

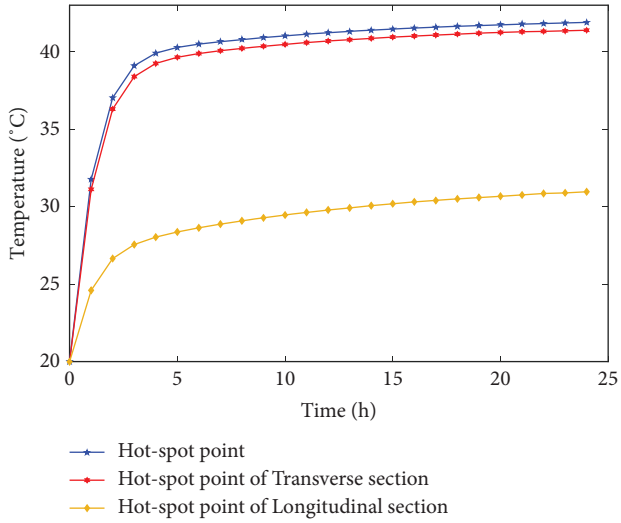

Figure 12: Temperature curve of sampling point (with firestop material).

the cable increases, it will inevitably lead to a further increase in the hot-spot temperature. In addition, only one of the many firestop materials used in engineering applications is discussed here. Since the firestop material blocks the heat dissipation effect of the air on the cable, other firestop materials may also increase the temperature rise, or even exceed the safe operating temperature. Therefore, it is essential to consider the influence of fire-blocking materials on the operating temperature of cables in engineering applications.

The cross-sectional results of the cable shaft at the position where the hot-spot temperature of the cable occurs are also obtained, as shown in Figure 11. Based on the results in Figures 5 and 11, it can be seen that the increase in the cable temperature will also lead to an increase in the air temperature inside the cable shaft.

The same positions are selected as the sampling points as in Figure 6, and the temperature curve of the power cable in the new model is also obtained, as shown in Figure 12. The simulation results show that, compared with the hot-spot point, the temperature increase near the power cable reflected by the sampling points in the transverse section is more obvious, but the change in the air temperature at the top of the lower shaft corresponding to the sampling points in the longitudinal section is relatively lower. In general, the temperature of the simulation results has increased as a whole, and the trend of temperature changes can be considered unchanged. Further, the fire-blocking material will cause a significant increase in the temperature of the cable in the surrounding area.

To further analyze the influence of fire-blocking materials on the simulation results, the curves of hot-spot temperature and air velocity are shown in Figure 13. The temperature increase caused by the firestop material will gradually increase with the increase of operating time. Although the flow rate of the surrounding air has

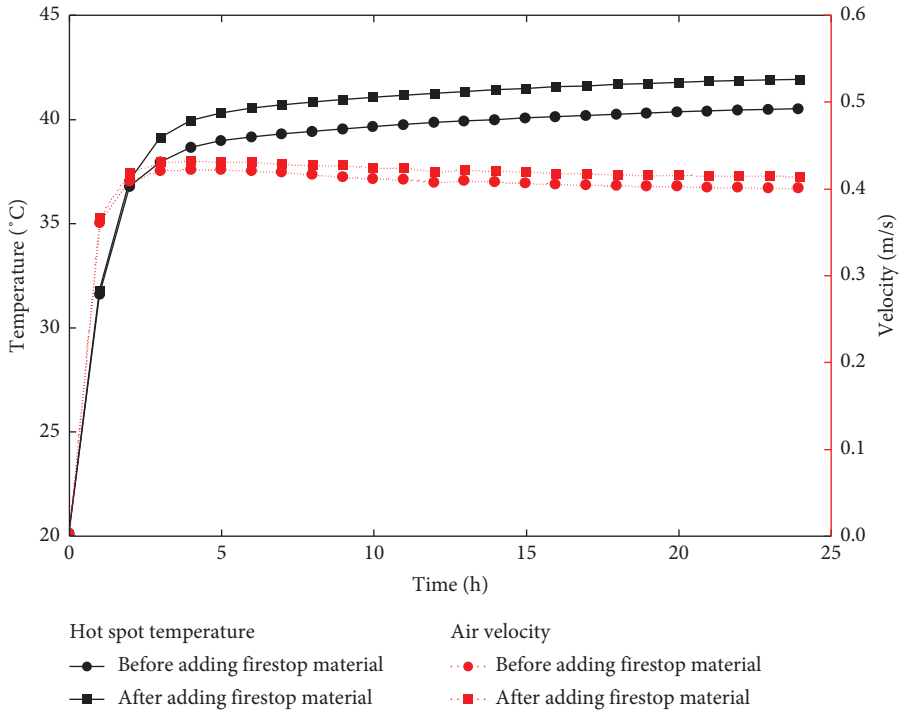

Figure 13: The influence of firestop material on hot-spot temperature and air flow rate.

also increased, this does not offset the damaging effect of the fire-blocking material on the heat dissipation of the cable.

6. Conclusion

Based on the theory of multiphysics analysis, this paper establishes a simulation model of a double-layer cable shaft. The electromagnetic-fluid-temperature field analysis of the cable shaft is carried out by using the direct coupling method, and the temperature and air velocity distribution inside the cable shaft are obtained. By comparing and analyzing the multiphysics simulation results before and after the use of fire-blocking materials, the following conclusions are as follows:

(i) Before using fire-blocking material, the hot-spot temperature of the cable under the rated condition is 40.5°C, and the hot-spot temperature rise is 20.5°C. The location appears near the floor of the lower cable, and it illustrates the effect of vertical laying mode on the operating temperature of the cable.

(ii) After adopting the fire-blocking material, the hot-spot temperature of the cable under the rated operating state will rise by 1.4°C. At the same time, the overall temperature distribution of the cable rises significantly, especially the temperature of the cable inside the firestop material, whose temperature rise exceeds 10.0°C.

(iii) It is essential to consider the effect of fire-resistant materials on the operating state of the cable in engineering applications, which will lead to a reduction in the current carrying capacity and safety performance of the power cable.

Data Availability

The data used to support the findings of this study are included in this paper and are available upon reasonable request.

Additional Points

This manuscript is conference extended paper, and the authors have cited this conference paper in literature [16]. The expansion work the authors have done on the basis of this conference paper includes: (i) The authors change the material property of air in the article from constant to variable that changes with temperature to increase the accuracy of simulation. (ii) The authors further analyzed the distribution of fluid field in the shaft. (iii) Different plugging materials are simulated to study the influence on fluid distribution and then study the influence on temperature distribution.

Conflicts of Interest

The authors declare that they have no conflicts of interest.

Acknowledgments

This work was supported by the State Grid Hubei Electric Power Co., Ltd. Shiyan Power Supply Company Technology Project (5215C02000RM).

References

[1] Q. Ma and W. Guo, "Discussion on the fire safety design of a high-rise building," *Procedia Engineering*, vol. 45, pp. 685–689, 2012.

[2] S. Ge, "China's high-rise building fire," *Fire Science and Technology*, vol. 29, no. 10, pp. 863–870, 2010.

[3] W. K. Chow, "Numerical studies on recent large high-rise building fire," *Journal of Architectural Engineering*, vol. 4, no. 2, pp. 65–74, 1998.

[4] S. Peng, S. Lu, and P. Lei, "Experimental study on perimeter fire barrier of a super-high building's glass curtain wall," *Fire Science and Technology*, vol. 37, no. 05, pp. 605–608, 2018.

[5] Z. Sun and Y. Zhou, "Discussion on fire-proof sealing technology and product," *Procedia Engineering*, vol. 135, pp. 644–648, 2016.

[6] Ministry of Emergency Management of the People's Republic of China, *Technical standard for application of firestop in building: GB 51410-2020*, Ministry of Emergency Management of the People's Republic of China, Beijing, China, 2020.

[7] Standardization Administration of the People's Republic of China, *Firestop Material: GB 23864—2009*, Standardization Administration of the People's Republic of China, Beijing, China, 2009.

[8] K. Wang, "Study on fireproof sealing treatment measures for high-rise building pipelines through walls or floor openings," *Urbanism and Architecture*, vol. 16, no. 02, pp. 61-62, 2019.

[9] J. Sun, L. Hu, and Y. Zhang, "A review on research of fire dynamics in high-rise buildings," *Theoretical and Applied Mechanics Letters*, vol. 3, no. 4, Article ID 042001, 2013.

[10] E. Ronchi and D. Nilsson, "Fire evacuation in high-rise buildings: a review of human behaviour and modelling research," *Fire Science Reviews*, vol. 2, no. 1, pp. 7–21, 2013.

[11] W. Guo, "Fire prevention and control of electric shaft," *Building Science*, vol. 30, no. 5, pp. 111–114, 2014.

[12] X. Miao, "Fire spread law of high-voltage cable channels in substations and improvement methods of fire blocking," Ph.M. Thesis, Shandong University, Qingdao, China, 2021.

[13] S. Liu, Y. Hu, and J. Zheng, "Dynamics simulation of 10kV cable tunnel fire for single-phase arc grounding fault," *High Voltage Engineering*, vol. 47, no. 12, pp. 4341–4348, 2021.

[14] R. Passalacqua, P. Cortes, N. Taylor, D. Beltran, P. Zavaleta, and S. Charbaut, "Experimental characterisation of ITER electric cables in postulated fire scenarios," *Fusion Engineering and Design*, vol. 88, no. 9-10, pp. 2650–2654, 2013.

[15] M. Wang, Y. Tian, and L. Yu, "Numerical simulation of the fire temperature distribution field and structural damages in an urban utility tunnel," *Modern Tunnelling Technology*, vol. 55, no. 5, pp. 159–165, 2018.

[16] B. Qu, X. Li, and X. Xiang, "Electromagnetic-fluid-temperature coupled field simulation on cable shaft in high-rise buildings," in *Proceedings of the 2022 IEEE International Conference on High Voltage Engineering and Applications (ICHVE)*, pp. 1–4, Chongqing, China, March, 2022.

[17] Y. Le, X. Zheng, and Z. Zhang, "Numerical calculation of ampacity for multiloop cable system in ducts based on electromagnetic-thermal-flow coupled field," *Science Technology and Engineering*, vol. 17, no. 05, pp. 197–202+261, 2017.

[18] C. Liao, J. Ruan, and H. Lu, "2-D coupled electromagnetic-fluid-thermal analysis of oil-immersed transformer," *Science Technology and Engineering*, vol. 14, no. 36, pp. 67–71, 2014.

[19] X. Zhao, H. Yifan, and G. Huang, "Calculation on steady-state current carrying capacity of intermediate joint of direct buried cable based on the finite element simulation," *High Voltage Apparatus*, vol. 58, no. 03, pp. 64–70+85, 2022.

[20] Q. Wang, G. Wang, and X. Chen, "Thermo-electric coupling simulation for 10 kV AC XLPE cable in DC operation," *Journal of Southwest Jiaotong University*, vol. 57, no. 01, pp. 46–54, 2022.

[21] J. He, J. Yang, and D. Ye, "Simulation and computation of temperature field and ampacity of conduit cable laying in different ways," *Electrical Measurement and Instrumentation*, vol. 53, no. 3, pp. 99–104, 2016.

[22] Y. Liang, Y. Li, and J. Chai, "A new method to calculate the steady-state temperature field and ampacity of underground cable system," *Transactions of China Electrotechnical Society*, vol. 22, no. 8, pp. 185–190, 2007.